University of Baghdad
College of Engineering
JOURNAL OF ENGINEERING

Journal of Engineering

journal homepage: www.joe.uobaghdad.edu.iq

Volume 29 Number 8 August 2023

3D- ABAQUS Modelling of Prestressed Concrete Hunched Beams with Multi-Openings of Different Shapes

Amjad Majeed Al-Hilali[1,*], Amer Farouk Izzet[2]

Department of Civil Engineering, College of Engineering, University of Baghdad, Baghdad, Iraq
a.thijeel1901p@coeng.uobaghdad.edu.iq[1], amer.f@coeng.uobaghdad.edu.iq[2]

ABSTRACT

A long-span Prestressed Concrete Hunched Beam with Multi-Opening has been developed as an alternative to steel structural elements. The commercial finite element package ABAQUS/CAE version 2019 has been utilized. This article has presented the results of three-dimensional numerical simulations investigating the flexural behaviour of existing experimental work of supported Prestressed Concrete Hunched Beams with multiple openings of varying shapes under static monotonic loads. Insertion openings in such a beam lead to concentrate stresses at the corners of these openings; as a result, extensive cracking would appear. Correlation between numerical models and empirical work has also been discussed regarding load displacement and crack development, and the obtained outcomes demonstrate a good agreement with the experiments. The ratio of ultimate loads and deflection of the beams tested in the investigation to those of numerical models was 0.98 and 0.97, respectively. So, finite element analysis can be regarded as a behaviour-trustworthy technique for simulating the non-linear behaviour of prestressed concrete rafters with multi-openings from the point of view of complexity, hardly, time-keeping, human effort, and cost.

Keywords: ABAQUS software, Prestressed Concrete, Finite Element (FE), Concrete Damaged Plasticity Model (CDPM), Hunched Beams.

*Corresponding author
Peer review under the responsibility of University of Baghdad.
https://doi.org/10.31026/j.eng.2023.08.11

Article received: 08/10/2022
Article accepted: 19/10/2022
Article published: 01/08/2023

نمذجة ABAQUS ثلاثية الأبعاد لعوارض متحدبة من الخرسانة سابقة الإجهاد مع فتحات متعددة بأشكال مختلفة

امجد مجيد ثجيل[1]،*، عامر فاروق عزت[2]

قسم الهندسة المدنية، كلية الهندسة، جامعة بغداد، بغداد، العراق

الخلاصة

تم تطوير الاعتاب الخرسانية سابقه الجهد المحدودبة التي تحوي العديد من الفتحات مستعرضه لتكون بديلا جيدا عن منشاءات الهياكل الحديدية لإسناد فضاءات كبيره. استخدامه حزمه العناصر المحددة التجارية *ABAQUS/CAE* ذات الاصدار 2019. قدمت الدراسة نتائج المحاكاة العددية ثلاثية الابعاد والتي اجريت لتحقق في سلوك الانثناء لعمل تجريبي مسند اسناد بسيط لا عتاب خرسانيه سابقه الجهد محودبه ذات فتحات مستعرضه متعددة وبأشكال مختلفة وتحت حمل ثابت ساكن. في الواقع وجود مثل هكذا نوع من الفتحات في هذه الانواع من الجسور يؤدي الى تركيز الإجهادات في زاويا الفتحات وبالتالي يولد تشققات ذات اعراض واسعه. تمت مناقشه العلاقة بين النماذج العددية والتحري التجريبي من حيث حمل الازاحات وتطوير التشققات مع الحمل واظهرت النتائج توافق جيد. حيث كانت نسبة الأحمال النهائية والهطول للأعتاب المختبرة في التحري التجريبي إلى تلك الخاصة بالنماذج العناصر المحددة العددية 0.98 و 0.97 على التوالي. لذلك ، يمكن اعتبار تحليل العناصر المحدودة أسلوبًا جديرًا بالثقة لمحاكاة السلوك غير الخطي للعوارض الخرسانية المحودبه سابقة الإجهاد ذات الفتحات المتعددة من وجهة نظر التعقيد وصعوبة وتوفير الوقت والجهد البشري والتكلفة.

الكلمات الرئيسية: برنامج ABAQUS ؛ الخرسانة سابقة الإجهاد؛ العناصر المحدود (FE) ؛ نموذج اللدونة التالفة للخرسانة (CDPM) ، الكمرات المحودبه.

1. INTRODUCTION

The advantages of Prestressed Concrete Hunched Beams (PCHBs) in industrial and bridge buildings, structural portal frames, and framed structures have been frequently utilized (**Hou et al., 2015)**. Instead of prismatic beams, these beams minimize the structure's weight, allowing for larger spans with no apparent reduction in loading capabilities **(Naik et al., 2017**). Researchers began looking for perforated RC rafters in the early sixties. (**Salam et al., 1977**; **Mansur et al., 1991**). Insertion openings in this type of beam have various advantages, including arithmetic flexibility, ease of shipment, and the construction of a structure where service pieces of machinery can pass during the web of beams, and, most importantly, the decrease in overall weight. Concrete is also relatively inexpensive and has good fire resistance (**Abdulkareem et al., 2022)**. It's also low-maintenance to support the roofs of warehouses, industrial facilities, and aeroplane hangars instead of steel parts (**Hassan et al., 2019a; Alkhafaji et al., 2020**).

On the other hand, insertion openings in such a beam lead to concentrate stresses at the corners of these openings; as a result, extensive cracking would appear (**Hassan et al., 2019b**; **Tu'ma et al., 2021**), which is unacceptable from both aesthetics and durability

standpoints. Consequently, the beam would be less rigid, leading to excessive deflections while under service loads. Because of this, the design of these beams need special treatment to keep the crack width under control and prevent the beam from failing prematurely (**Mansur et al., 1999; Sahi et al., 2021**). Since concrete lacks significant tensile strength, creating long-span beams is challenging. To bypass this problem, prestressed reinforcement was required, as achieving the required span lengths with ordinary reinforcement was impossible (**Samir et al., 2013; Al-Hilali et al., 2022a**). Al-Hilali and others investigated the short-term deflection of prestressed concrete hunched beams with various opening configurations (**Al-Hilali et al., 2022b)**. The parametrical examinations of this research were the opening configurations (quadrilateral or circle) and the chord depths. It was found that specimens with round holes were stiffer when loaded than those with trapezoidal holes. Furthermore, rafters with inclined posts and trapezoidal holes were stiffer than beams with vertical posts. They examine the performance of prestressed concrete hunched beams with multi-openings of different shapes PCHB systems by conducting a numerical analysis of a commercial version of ABAQUS/CAE 2019. This is a flexible analysis tool that may be used to address both linear and non-linear problems. Additionally, ABAQUS is a robust numerical gadget often used for modelling. But the performance of concrete is sophisticated, and several factors must be considered for analysis, in which concrete experiences stiffness degradation and strain-softening in both compression and tension (**Lubinar et al., 1989**). The ABAQUS software's Concrete Damage Plasticity Model (CDPM) has been introduced to fit the earlier behaviour of concrete and other quasi-brittle materials. The degradation process in the elastic stiffness is expressed in the damage parameters dc and dt, illustrated in **Fig. 1** for compression and tension, respectively.

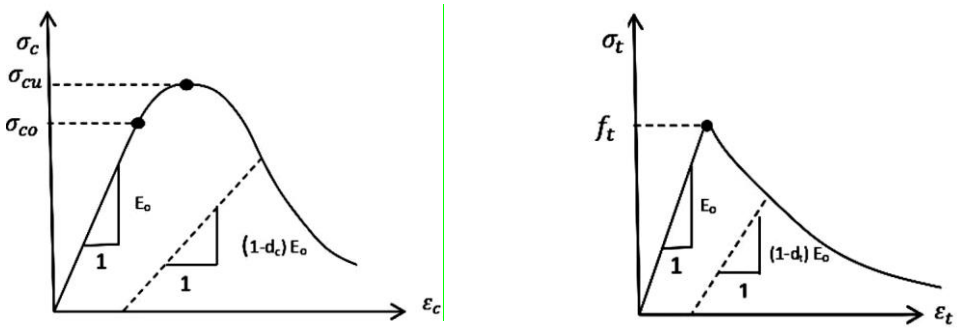

(a) **(b)**

Figure 1. Behaviours of concrete: (a) uniaxial compression, (b) uniaxial tension. **(ABAQUSE User Manual, 2019).**

(Amiri et al., 2004) investigated the effect circular openings have on the behaviour of structural concrete beams. Under a four-point load, nine regular concrete beams with openings, five high-strength concrete beams with openings, and one beam as a reference solid with normal concrete were evaluated. The most important discovery was that the ultimate strength decreased, and cracking was enlarged in normal concrete beams when the diameter of the aperture surpassed one-third of the beam's depth. This was the case in all of the beams tested. At the same time, the diameter and the position of the aperture are the primary parameters that influence the strength of the concrete**.** Later, **(Al-Shaarbaf et al.**, **2007**) introduced a three-dimensional "Finite Element Model" that can simulate the flexural behaviour of concrete beams with only one rectangular opening. Validation was carried out using numerous models, including a rectangular transverse opening demonstrating a good

agreement between the experimental and numerical findings. The significant factors studied on the structural behaviour of the member were the concrete strength, reinforcing ratio, and opening size. Ultimate strength and post-cracking stiffness for beams increased when the amount of bottom reinforcement and the concrete strength increased but decreased with increasing opening size. **(Madkour et al., 2007)** suggested a modern theory of non-linear three-dimensional elastic damage to model the deformation of the reinforced concrete (RC) beam. The simulation of the non-linear behaviour of RC beams with openings based on thermodynamics was given more attention. The non-linear elastic behavior and the degraded condition of concrete materials are taken into account in the suggested theoretical method. The provided non-linear concrete model has been validated using a series of numerical simulations of experiments analyzing the behaviour of reinforced concrete beams subjected to monotonic static loads. The experimental data presented in the literature were compared with the suggested model, and a good agreement was found. To comprehend the behavior of concrete, several researchers have constructed constitutive models (**Park and Paulay, 1975; Scott et al., 1982; Wang and Hsu, 2001; Seow and Swaddiwudhipong, 2005**). But although there are many of these methods, several areas still need further investigation. Based on the input information, notably the material properties, finite element (FE) software may perform a realistic analysis of structures. Concrete is widely utilized in the construction industry, although it is highly non-linear under uniaxial compression as a composite material. As a result of its brittle behaviour. So, Concrete fails to crack under tension and crushes under compression. Concrete failure modelling has become a concern in modern concrete structures.

This study investigates the serviceability (deformability and cracking) Of Perforated Prestressed Concrete Haunched Beams (PPCHBs) subjected to external concentrated load at mid-span. Adopting this work finds the optimum model of PPCHBs depending on the correlation between the covered variables, namely: number, size, the configuration of the openings, and inclination of the posts, and the maximum load-carrying capacity.

2. FINITE ELEMENT MODEL

2.1 Geometrical Modeling

Describing the geometric elements of the tested specimen is the beginning stage in finite element modelling. **Fig. 2** depicts the finite element idealization for the tested beam under static loading, which includes all beam components.

2.2 Material Modeling

Under all stress states, excluding the hydrostatic pressure, concrete experiences stiffness degradation and strain-softening in compression and tension (**Lubinar et al., 1989**). The Concrete Damage Plasticity Model (CDPM) in the Abaqus software has been introduced to fit the earlier behaviour of concrete and other quasi-brittle materials. The degradation process in the elastic stiffness is expressed in the damage parameters *dc* and *dt*, illustrated in **Fig. 1** for compression and tension, respectively. The damage parameters are complicated to be mathematically expressed.

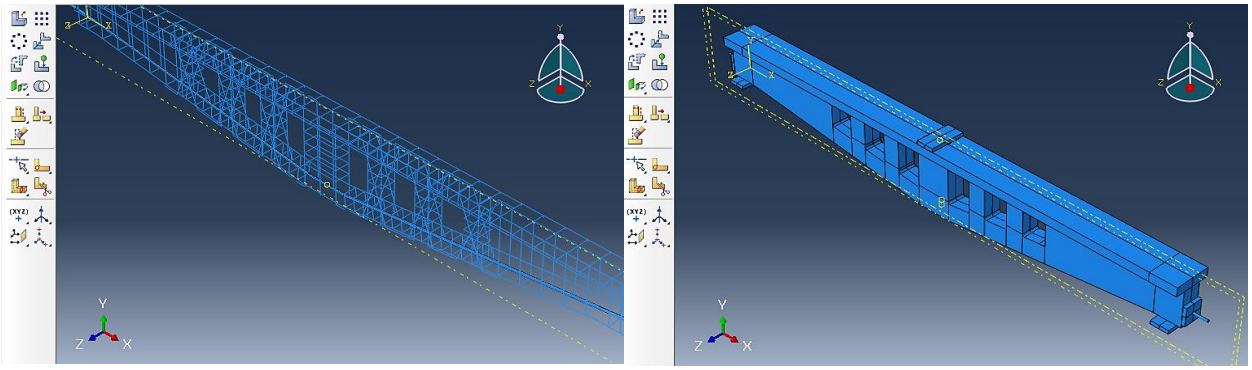

(a) (b)

Figure 2. Finite element idealization of concrete hunched beams with multi-openings (a) Reinforcements bars (b) All geometry parts modelling, support, load, end plates modelling

However, (**Hafezolghorani et al., 2017**) introduced a simplified expression for the parameters dc and dt. According to the proposed model, the parameters are evaluated using Eq. (1), and no damage occurs in the stiffness before the apex of the stress-strain curve.

$$d_{c,t} = 1 - \frac{\sigma_{c,t}}{\sigma_{u\,c,t}} \quad (1)$$

where; σ is the stress in concrete (N/m^2), σ_u is the ultimate stress (N/m^2), and the subscripts c and t refer to compression and tension, respectively.
In tension, σ_u=f_t. This formula is used in the current study to evaluate and define the damage parameters dc (compression deformation) and dt (tensile deformation).
To determine the plasticity characteristics of concrete, the (CDPM) model needs five plasticity parameters, primarily:

1. Dilation angle (ψ): it is the internal friction angle of the material or, in other words, the increase in concrete's plastic volume is more than the value of critical stress. (**ABAQUS User Manual, 2013**). As a rule of thumb, ψ = 20° to 40° is suggested in simulations, which affects the material's flexibility. As a result, the dilation angle profoundly impacted the entire model. An increase in the dilation angle increased the system's flexibility. (**Hafezolghorani et al., 2017**). However, recent research has successfully employed larger values of ψ. A value of =56^o was chosen for use with reinforced concrete (**Demir et al., 2016**). For reinforced and post-tensioned concrete slabs, (**Huang et al., 2010**) decided to use ψ =50^o. After doing several analyses, the optimal value for this study was found to be 40^o.
2. The flow potential eccentricity (ς): this parameter can be defined, according to (**Jankowiak and Odygowski, 2005**), as a ratio of tensile strength to compressive strength. The flow potential eccentricity is set to 0.1 by default. Raising this value increased the flow potential's curvature **(Hafezolghorani et al., 2017)**.
3. The ratio of the biaxial compressive to the uniaxial compression stress for concrete ($\frac{f_{c,biaxial}}{f_{c,uniaxial}}$): a parameter that defines the point at which the material fails under biaxial compression. A ratio of 1.16 was adopted.

4. Kc Parameter: the ratio of the second stress invariant on the tensile meridian,$q(TM)$, to that on the compressive meridian, $q(CM)$. The default value is $2/3$ was adopted in this research.
5. The viscoplastic regularization parameter (μ): is a parameter that is necessary for the viscoplastic regularization of the model. This parameter improved the model's convergence rate during softening, resulting in favourable outcomes. In the present study, the value of μ = 0.0004 was adopted.

2.2.1 Compressive Behavior of Concrete

Uniaxial compressive behaviour can be defined by an existing constitutive model proposed by (**Hognestad, 1951**) (i.e., the stress-strain relationship of concrete), as shown in **Fig. 3** and suggested in Eq. (2), which has been adopted in this simulation**.**

$$\sigma_c = f_c^{'}\left[2\left(\frac{\varepsilon_c}{\varepsilon_o}\right) - \left(\frac{\varepsilon_c}{\varepsilon_o}\right)^2\right], \varepsilon_o = \frac{2f_c^{'}}{E_c} \quad (2)$$

where; σ_c nominal concrete compressive stress (MPa). E_c: Modulus of elasticity of concrete (MPa). $f_c^{'}$: Maximum compressive strength of concrete (the unconfined cylinder specimen) (MPa). ε_c : nominal compressive strain in concrete. ε_o : Strain at maximum stress (the strain at the curve's peak point). From beginning to end, the equation for the non-linear behaviour of concrete was assumed.

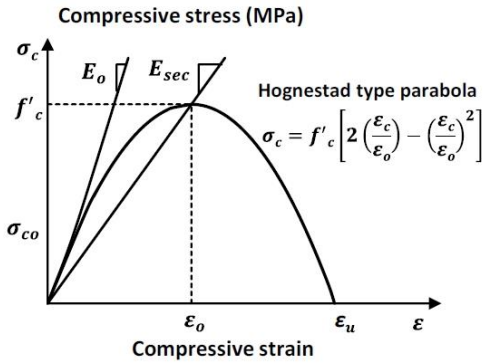

Figure 3. Hognestad Parabola (**Hognestad, 1951**)

This study assumed the linear part is deemed up to a stress of 0.40. The modulus of elasticity of concrete (E_o) is equal to the secant modulus of elasticity; specifically, it is the inclination of the line segment between the starting point and the point on the curve at which the stress is $0.40f_c^{'}$. A concrete crushing strain of 0.0035 was adopted in agreement with the range in the ACI code commentary (0.003-0.004) (**ACI Committee 318, 2019**). The inelastic strain was calculated according to Eq. (3) (**Hafezolghorani et al., 2017**):

$$\varepsilon_c^{in} = \varepsilon_c - \frac{\sigma_c}{E_o} \quad (3)$$

Damage caused by increased plastic strains in semi-brittle materials is shown as a reduction in the curve's tangent concerning the initial diamond (modulus of elasticity, E_o), as seen in **Fig. 1**. At the curve's apex (i.e., ultimate compressive stress $f_c^{'}$), the damage parameter (dc) was zero; then, it gradually decreased to 0.8, concerning 20% remaining strength in big strain. (**Hafezolghorani et al., 2017**).

2.2.2 Tensile Behavior of Concrete

Concrete subjected to tension is not regarded as a brittle-elastic form, and such phenomena as aggregate interlocking inside cracks and concrete-steel adhesion amidst cracks are considered. Therefore, the stress-strain drop in the tension zone does not occur suddenly but is relatively progressive. The Finite Element (FE) analysis results for RC concrete structures are highly sensitive to the user-defined parameters of tension stiffening. These parameters are the ultimate tensile stress and ultimate cracking strain. The post-failure strain softening of the tensile stress demonstrated in **Fig. 1b** can be approximated to linearly vary from the maximum tensile stress (ft) at failure strain ($\varepsilon_{cr,failure}$) to zero at the ultimate total cracking strain (ε_{ucr}). Thus, (ε_{ucr}) is the total cracking strain at which a complete loss of tensile strength is reached. According to (**Reddiar, 2010**), this strain is one-tenth that corresponding in compression (ε_{cu}), and ε_{cu} is evaluated according to Eq. (4):

$$\varepsilon_{cu} = 0.012 - 0.0001 f_c' \ (in\ MPa) \quad (4)$$

when; $f_c^{'} = 45$ MPa, for instance, ε_{ucr} will be 7.5×10^{-4}. While this value, according to estimating (**Abaqus analysis user's manual**,**2013**) ε_{ucr} about 10×10^{-4}. The inelastic cracking strain (ε_{incr}) that should be defined as not the total strain but after deducing the failure strain (f_t/E_o). Again, the manual suggests starting the analysis with a failure strain of 1×10^{-4}. Hence, the ultimate ε_{cr} will be 7.5×10^{-4}; it is 7.5-times $\varepsilon_{cr,failure}$. The ultimate cracking strain ε_{cr} adopted in the current modelling is taken equal to 7.5 $\varepsilon_{cr,failure,}$. (**Alkloub et al. 2019**) used an ultimate cracking strain of 0.00154, while the strain at failure calculated from the material properties is ($3.86/22960 = 1.68 \times 10^{-4}$); it is 9.16-times $\varepsilon_{cr,failure}$. At any point, the cracking strain ε_{cr} is evaluated according to Eq. (5):

$$\varepsilon_{cr} = \varepsilon_t - \frac{\sigma_t}{E_O} \quad (5)$$

As mentioned in the ABAQUS analysis user manual, increasing the values of the tension stiffening parameters enables FE solutions. In contrast, using too few values results in a local cracking failure, which causes unstable behaviour. The input data (material properties) for concrete with the CDPM were carried out in tabular format, as shown in **Table 1**.

2.2.3 Reinforcement Steel Modeling Properties

The reinforcements and stirrups steel has been modelled numerically as elastic-perfectly plastic depending on the von mises failure, which considers the material elastic behaviour up to the yield stresses and, after this point, becomes completely plastic, as shown in **Fig. 4** (**ABAQUS User Manual, 2013**). The modulus of elasticity and Poisson's ratio of the reinforcement material are the two factors that determine the linear isotropic portion, which has been taken as 200×10^3 MPa, and 0.3, respectively. As presented in the experimental test, the bilinear isotropic portion is defined via yield stress. Also, the steel bearing and support plates are simulated as linear isotropic substances. The reinforcement material uses the same values to simulate linear isotropic for both the modulus of elasticity and Poisson's ratios 200×10^3 MPa and 0.3, respectively. The prestressing steel was modelled as multilinear isotropic material. The modulus of elasticity of the strand and Poisson's ratio are 197.5×10^3 MPa and 0.3, respectively.

Table 1. Input data for Concrete Material properties.

Material's parameters		Plasticity parameters	
		Dilation angle	40
Concrete elasticity		Eccentricity	0.1
Young's modulus (E)	28900	f_{bo}/f_{cbc}	1.16
Poisson's ratio (υ)	0.2	k	0.67
		Viscosity parameter	0.0004
Concrete compressive behaviour		Concrete compression damage	
Yield stress (MPa)	Inelastic strain	Damage parameter (dc)	Inelastic strain
20.5	0	0	0
26	0.000033	0	0.000033
30.7	0.000088	0	0.000088
34.8	0.000159	0	0.000159
38.2	0.000247	0	0.000247
41	0.000353	0	0.000353
43	0.000476	0	0.000476
44.3	0.000617	0	0.000617
45	0.000776	0	0.000776
44.8	0.000952	0.00108	0.000952
44.1	0.001146	0.017509	0.001146
42.7	0.001357	0.049273	0.001357
40.6	0.001586	0.0963713	0.001586
37.8	0.001833	0.1588033	0.001833
34.3	0.002097	0.2365703	0.002097
30.1	0.002379	0.3296713	0.002379
25.2	0.002679	0.4381073	0.002679
19.6875	0.002996	0.5618763	0.002996
Concrete tensile behaviour		Concrete tension damage	
Yield stress (MPa)	Cracking strain	Damage parameter (dt)	Cracking strain
6.92	0	0	0
0.00	0.0024	0.99	0.0024

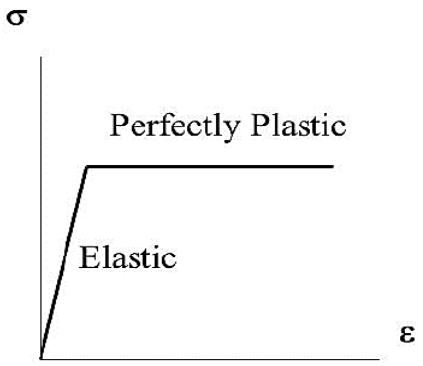

Figure 4. Stress-strain curve of the reinforcing steel

2.2.4 Load Application and Boundary Conditions

In the simulation, the boundary conditions and the external load application were identical to those utilized in the experimental tests. One of the support structures was represented as a hinge, while the other was modelled as a roller. (Ux=Uy=Uz=0) was used to ensure the constraining of one of the supports and act as the hinge. And it permitted longitudinal displacements and rotations toward the x-axis while simultaneously restricting the y and z directions (Uy=Uz=0), achieving modelled roller support, see **Fig. 5**. The numerical model was initially subjected to the recorded prestressing strand force in a solitary step of loading (step No.1). The effective stress for the strand was used as the pressure applied in the x-direction during the prestressing process utilizing a predefined field. The tested beam's self-weight wasn't considered, while in (step No.2) of modelling, The load was added to the steel loading plate in the second step.

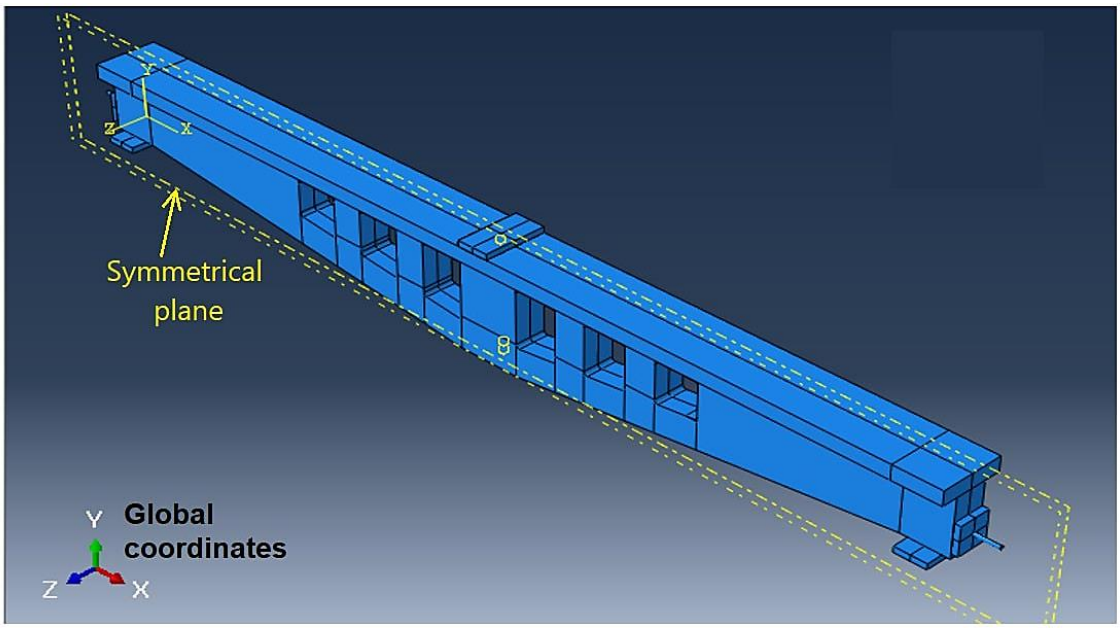

Figure 5. Location of induced displacement and boundary conditions

2.2.5 Meshing of the Model

The mesh module includes tools that allow the creation of meshes on the parts and assemblies that have been formed. Many available elements in ABAQUS software can be utilized, and choosing the appropriate element that suits the problem well is essential. The non-prismatic perforated prestressed concrete beams (NPPCBs) are modelled in 3D stress elements for all model components except steel reinforcements, which utilize standard 2D features. These elements provide appropriate integration standards based on the empirical response of the specimen. The maximum approximate size was 20 mm for concrete meshing, 40mm for end and support plates, and 40 mm for reinforcements (mild steel and tendons). The reinforcement steel may be simulated by solid or truss elements.
The solid elements are complex arithmetically, so they are not chosen. Since reinforcement bars don't have a high flexural stiffer, truss elements, have been used and modelled as embedded elements, and their bond to concrete is to be completely bonded. Linear brick hexahedral C3D8R elements are continuum elements (C) having 3D eight nodes (8) with

reduced integration (R) and were selected for the finite element models for concrete beam, support plates, end bearing plates, and strand volumes. In comparison, T3D2 elements are element (T) having 2D two nodes (2) were selected for the finite element models for Steel reinforcing bars (longitudinal and shear reinforcement). **Fig. 6** and **Table 3** show T3D2 and C3D8R elements.

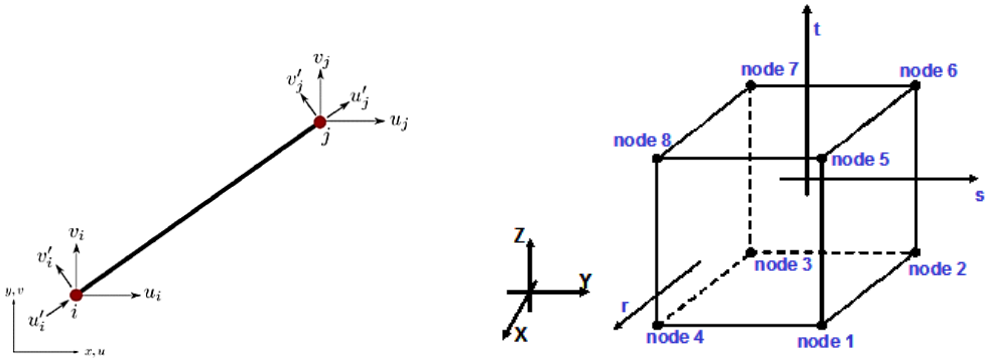

T3D2 (2-node linear 3D truss) element C3D8R (8-node solid 3D) element

Figure 6. Finite element type used for modelling

Table 4. Description of the used elements

Beam components	Family	Element characteristics
Concrete, strand, and bearing steel plates	3D Stress	C3D8R: A continuum, three-dimensional, 8-node linear brick, reduced integration, hourglass control
Steel reinforcing bars	Truss	T3D2: A tie, three-dimensional, 2-node linear truss

3. EXPERIMENTAL STUDY AND DETAILS OF THE TESTED BEAMS

This section briefly explains the experiment works, including the tested setup and some important conclusions. Details of the empirical study have been published in other publications (**Al-Hilali et al., 2022b**). Six prestressed concrete hunched beams with multi openings of different configurations and one control specimen (i.e., solid) as a standard beam under monotonic static loading mid-span till failure. A variable that was considered was the number of openings and their height.

The tested beams had the same type, size, and dimensions, with a total span of 3000 mm and an exact clear length of 2850 mm. The depth of the mid-span beam is 400 mm, while the depth of the end-section beam is 250 mm (i.e., the depth of the beams diminished as they approached the support). The web width for the beam was 100 mm, the width of the flange was 200 mm, and the depth of the flange was 50 mm. The openings are identified by posts that are 100 mm wide. **Figs. 1 and 2** show that the necessary reinforcement details included short stirrups in chords, additional diagonal bars around openings, the posts, and full-depth stirrups next to openings and prestressing strands. Based on the variables, specimens have been divided into three groups (A, B, and C), as seen in **Table 5**.

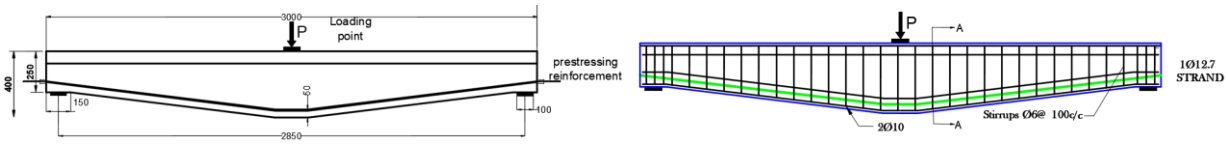

a) Schematic layout and details of steel reinforcement of beam PB

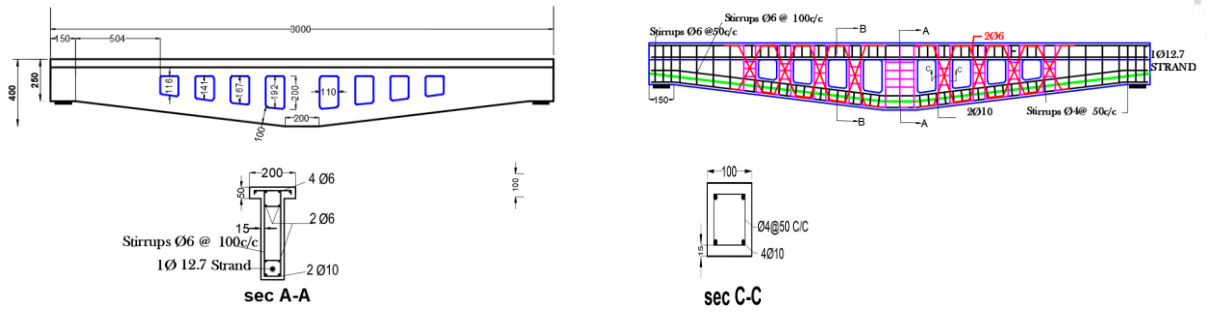

b) Schematic layout and details of steel reinforcement of beam PQ8

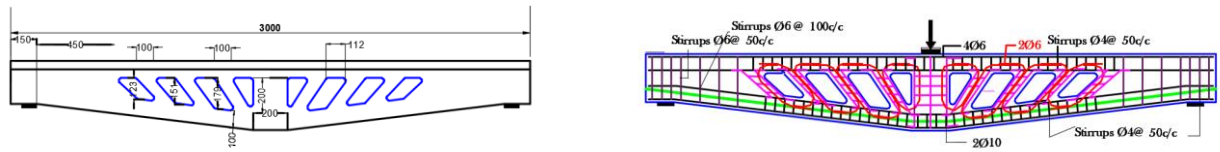

c) Schematic layout and details of steel reinforcement of beam PQI8

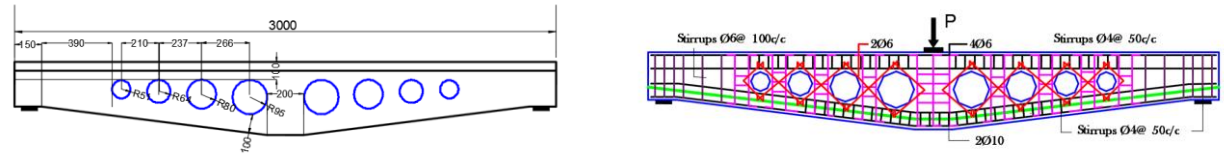

d) Schematic layout and details of steel reinforcement of beam PC8

Figure 7. Schematic layout and details of steel reinforcement for all specimens. (Note: All dimensions in mm)

Table 5. Details of the tested beams

Group	Beam ID*	Shape of openings	Number of openings	The total area of openings (mm^2)	Upper chord height (mm)	Lower chord height (mm)
solid beam	PB	------	-------		----	-----
A	PQH8	Quadrilateral with vertical post	8	180000	75	75
	PCH8	Circular	8	228000	75	75
B	PQ8	Quadrilateral with vertical post	8	139000	100	100
	PC8	Circular	8	139000	100	100
C	PQI8	Quadrilateral with inclined posts	8	139000	100	100
	PC8	Circular	8	139000	100	100

* P: Prestressed, B: Beam, H: Height of chord 75, Q: Quadrilateral, C: Circular, I: Inclined posts, 8: Number of openings.

The materials properties utilized in this study are summarized in **Table 6**. Cement, coarse-aggregate, and fine-aggregate were tested in accordance with Iraqi standards (IQS), whereas mild steel reinforcement was tested in accordance with ASTM standards. They were using a 7-wire strand with a 0.5 (in) diameter (Grade 270), and a post-tensioning jacking force of (110kN) was supplied from one end in accordance with the requirements of **ACI-318M-19**.

Table 6. Material properties.

Material	Diameter [mm]	Yield stress [MPa]	Average compressive strength f_c' [MPa]	Average ultimate tensile strength [MPa]	Average modulus of elasticity [GPa]
strand	12.7	1674	------	1860	197.5
rebar	10	600	------	678	200
	6	550	------	670	200
	4	410	------	516	200
Concrete	------	------	45	4.36	28.9
Note: Results represent the average of three control specimens.					

4. PRESENTING AND DISCUSSING THE OUTPUTS OF NUMERICAL ANALYSIS.

The results of the experiments on the tested beams were used as a verification problem and then compared to the numerical analysis outcomes for all tested specimens. In FEM analysis, all of the models use static analysis. **Fig. 8** shows the Stress component at the integration point shape of one of the beams that have been analyzed.

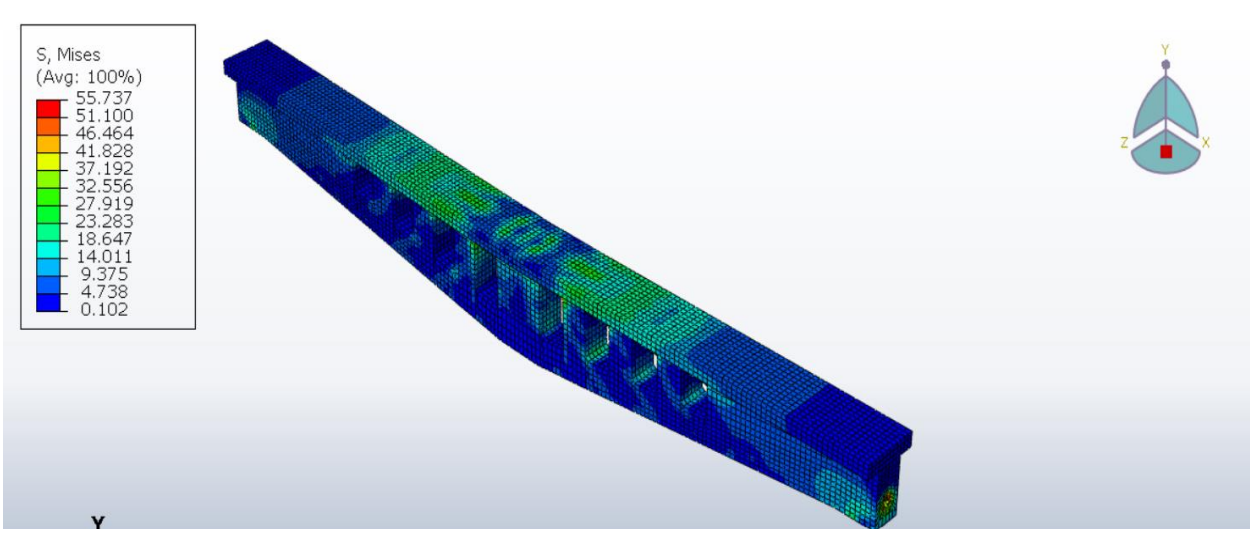

Figure 8. Stress component at integration points distribution shape for beam PQ8

4.1 The Camber in the Tested Beams

Table 7 compares the tested beams' camber at mid-span obtained from the experimental work and the finite element model at the prestressing force transfer. Good agreement was obtained between the camber of numerical models and found experimentally where the

value of the average and coefficient of variation for $(\delta w)_{FE.} / (\delta w)_{Ex}$ was (0.89) and (8.6) %, respectively. Based on the results of the FE analysis, it may be seen that the simulated models are stiffer than the tested experimental results. Several factors could cause the FEM analysis results to show a higher stiffness. During the experiment, Microcracks cracks were found in the concrete, caused by drying shrinkage and treating environmental conditions. These factors would make the actual specimens less stiff. There is no way to model these microcracks cracks in finite element models. In a finite element analysis, an ideal bond is assumed to exist between the concrete and the steel reinforcing. The actual specimen will not wholly match this assumption. The composite work between the concrete and steel reinforcement is lost when a bond slip occurs. This means the FE analysis's predicted stiffness may be higher than the actual specimen's total stiffness (**Kmiecik et al., 2011**). **Fig. 9** shows the shape of one of the camber in a beam that has been analyzed.

Figure 9. Camber in beam PQ8 (deformation unit in mm).

Table 7. Comparison of the camber at mid-span.

Group	Beam ID	Camber at mid-span section $(\delta w)_{Exp.}$ (mm)	Camber at mid-span section $(\delta w)_{FE.}$ (mm)	$(\delta w)_{FE.} / (\delta w)_{Ex}$
Solid beam	PB	0.88	0.86	0.97
A	PQH8	1.32	1.10	0.83
	PCH8	1.18	1.05	0.89
B	PQ8	1.20	0.95	0.79
	PC8	0.95	0.92	0.97
C	PQI8	1.09	0.92	0.84
	PC8	0.95	0.92	0.97
			Mean	0.89
			Standard deviation	0.077
			C.O. V	8.6%

4.2 Loads and Deflection at the Ultimate Stage

The numerical model addresses concrete's most basic phenomena based on the modified Mohr-Coulomb models. It was established to probe the impact of damage caused by mechanisms of failure in the substance. **Table 8** compares the ultimate loads, the deflection at mid-span produced using the FE model, and the empirical works done at the final phase for all tested beams subjected to static testing. There was a good agreement between numerical simulations' failure loads, maximum displacement, and empirically tested outcomes. With the mean value and C.O.V for maximum loads $(Pu)FE/\ (Pu)Exp$ being 0.98 and 2.34%, respectively, and the average value and coefficient of variation for mid-span deflection $(\delta FE/\delta Exp)$ being 0.97 and 6.43%, respectively. **Fig. 10** shows the shape of one of the displacement distributions in a beam that has been analyzed.

Table 8. Comparison of the failure load and mid-span deflection.

Groups	*Beam ID*	*Failure Load kN*		$\frac{(Pu)FE}{(Pu)Exp}$	*Mid-span deflection(mm)*		$\frac{\delta\ FE}{\delta\ Exp}$
		(Pu)Exp	(Pu) FE		δExp	δFE	
solid beam	PB	163.8	155.7	0.95	30	31.3	1.04
A	PQH8	146.3	144.2	0.98	41.2	35.5	0.86
	PCH8	152.4	154.2	1.01	40.25	37.98	0.94
B	PQ8	153.7	154.4	1.00	41	40.41	0.98
	PC8	160	154.8	0.97	40	40.9	1.02
C	PQI8	152.4	155.2	1.01	37.5	35.47	0.95
	PC8	160	154.8	0.97	40	40.9	1.02
Mean				0.98	*Mean*		0.97
c. o. v				2.34%	c. o. v		6.43%

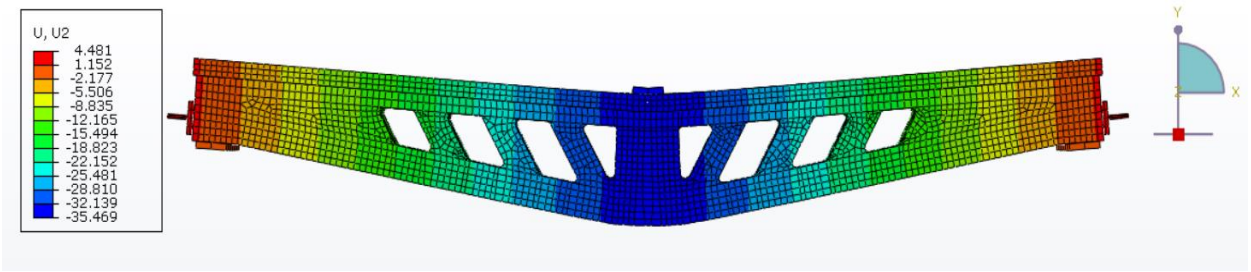

Figure 10. Displacement distribution in the beam PQI8 (unit of deformation in mm).

4.3 Load-Deflection

For ABAQUS, the deflections for the experimental beams are recorded at mid-span. The load-deflection curves obtained from the finite element analyses are compared with the experimental results for test beams, as seen in **Fig. 11**.

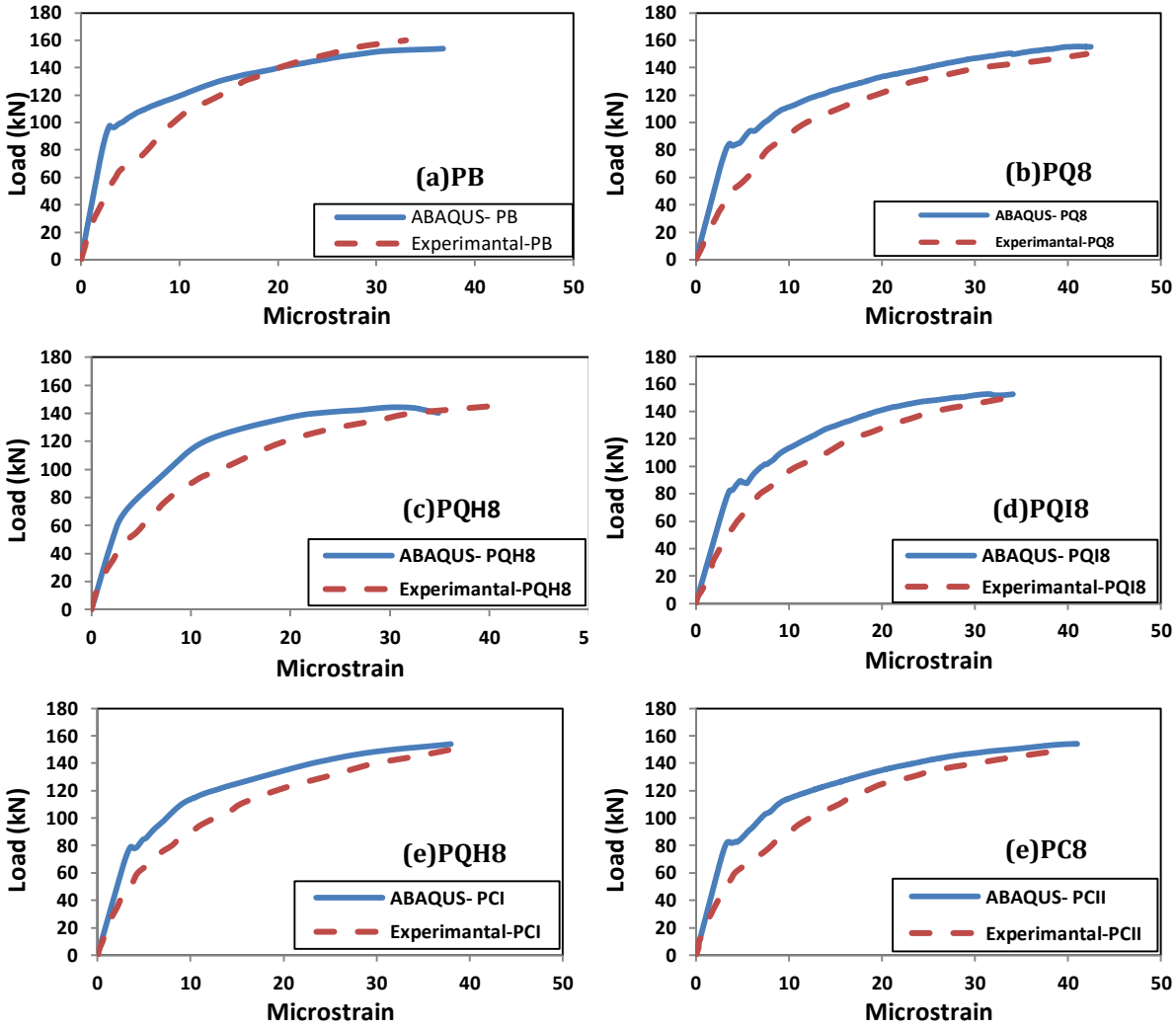

Figure 11. Experimental and numerical load-deflection comparison for the analyzed beams.

It can be noticed that the experimental and numerical load-deflection curves have a similar trend and pretty well with the experimental data for all tested beams, however, the load-deflection responses of the finite element studies for all beams are significantly more rigid than those of the experimental results and for the same reasons mentioned in section 4.1.

4.4 Crack Pattern

Based on the CDPM theory, cracks in RC elements are generally formed in regions where the tensile strain occurs exceeds the limited tensile strain in concrete (i.e., the plastic stress for concrete exceeds zero). Therefore (DAMAGE T) damage in tension was utilized as a substitution for crack growth in the flexural zone in the current study. The cracks' orientation is perpendicular to the utmost main plastic strain. In general, diagonal tensile cracks at the corners of the openings occurred early. When the applied loads increased, vertical tension cracks spread along the lower chord, and flexural cracks appeared; this can be monitored in ABAQUS software by navigating between the increments in the second step from loading. **Figs. 12-16** display a contour plot of the (DAMAGE T) damage in tension in the

analyzed simulation to the crack patterns of the empirical works for tested specimens at the final stage; this depicts the impact of apertures on stress concentrations and the formation of cracks. Based on these figures, stress concentrations occurred at the corners of the apertures and the lower tension chords. Also, an excellent coincidental crack pattern between the numerical and experimental work can be observed.

(a)

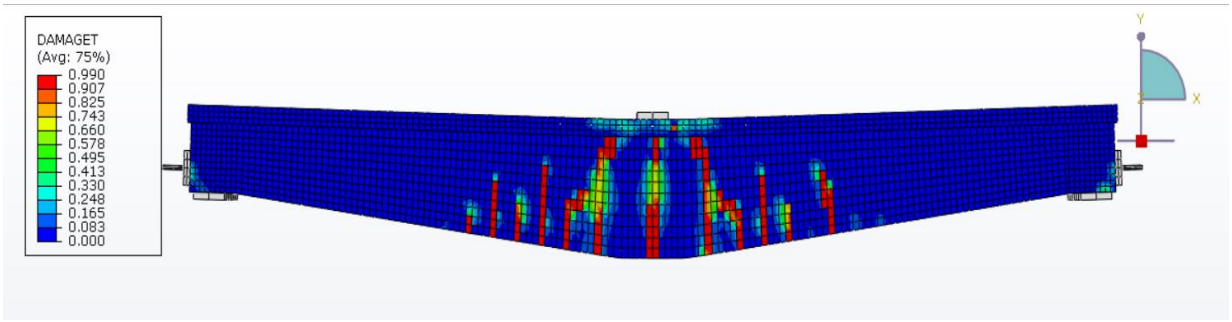

(b)

Figure 12. The results of the analysis for the (PB) FE model: (a) Cracks failure as in the picture, (b) damage in tension (flexural cracks), MPa

(a)

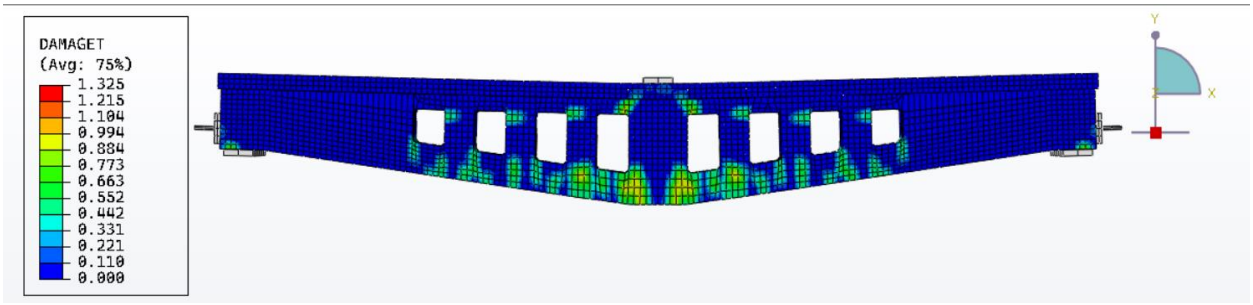

(b)

Figure 13. The results of the analysis for the (PQ8) FE model: (a) Cracks failure as in the picture, (b) damage in tension (flexural cracks), MPa

(a)

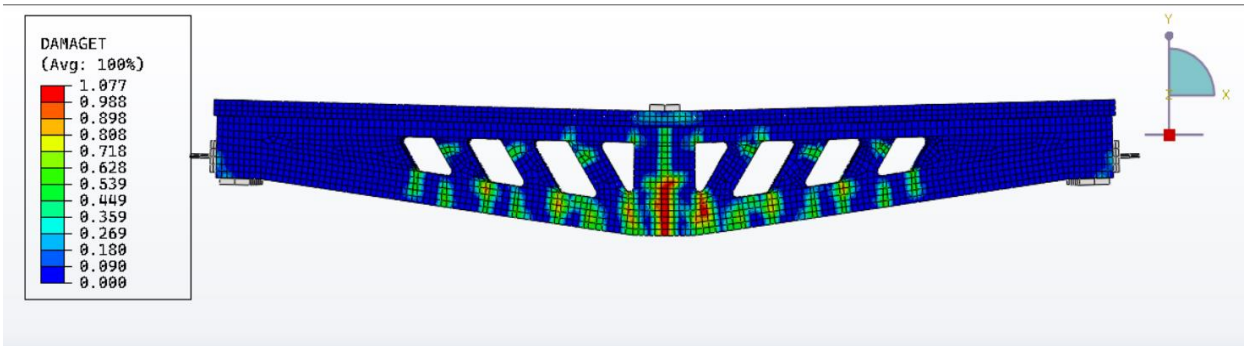

(b)

Figure 14. The results of the analysis for the (PQI8) FE model: (a) Cracks failure as in the picture, (b) damage in tension (flexural cracks), MPa

(a)

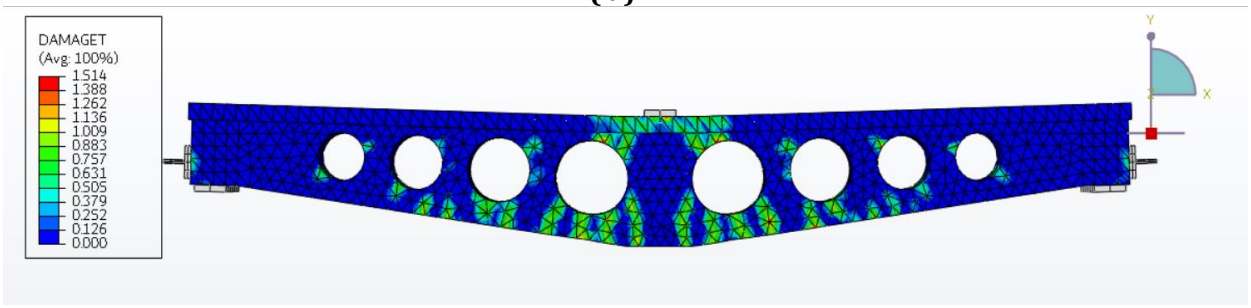

(b)

Figure 15. The results of the analysis for the (PCH8) FE model: (a) Cracks failure as in the picture, (b) damage in tension (flexural cracks), MPa

(a)

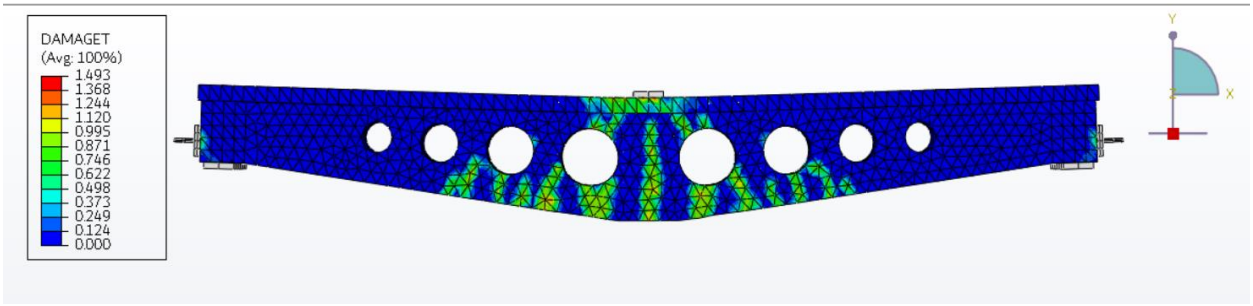

(b)

Figure 16. The results of the analysis for the (PC8) FE model: (a) Cracks failure as in the picture, (b) damage in tension (flexural cracks), MPa

4.5 Stress Distribution along the Beams' Main Reinforcement

The stresses in the longitudinal primary reinforcement (steel and tendon) at the tension chord are shown in **Fig. 17** for the three phases of loadings (40 KN, 80 KN, and ultimate loads).

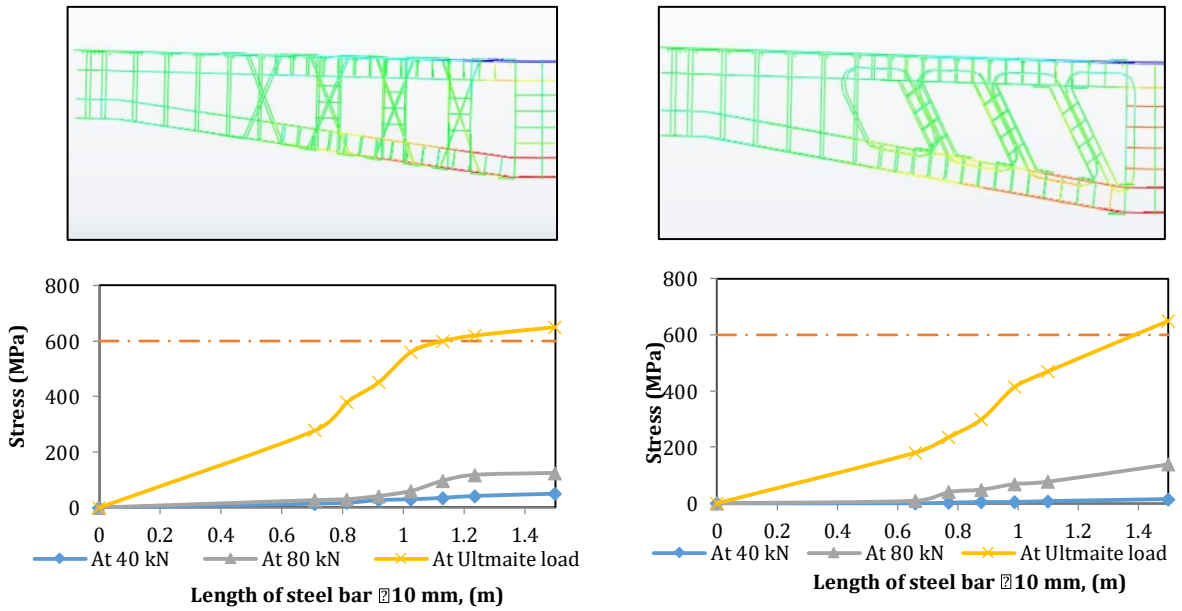

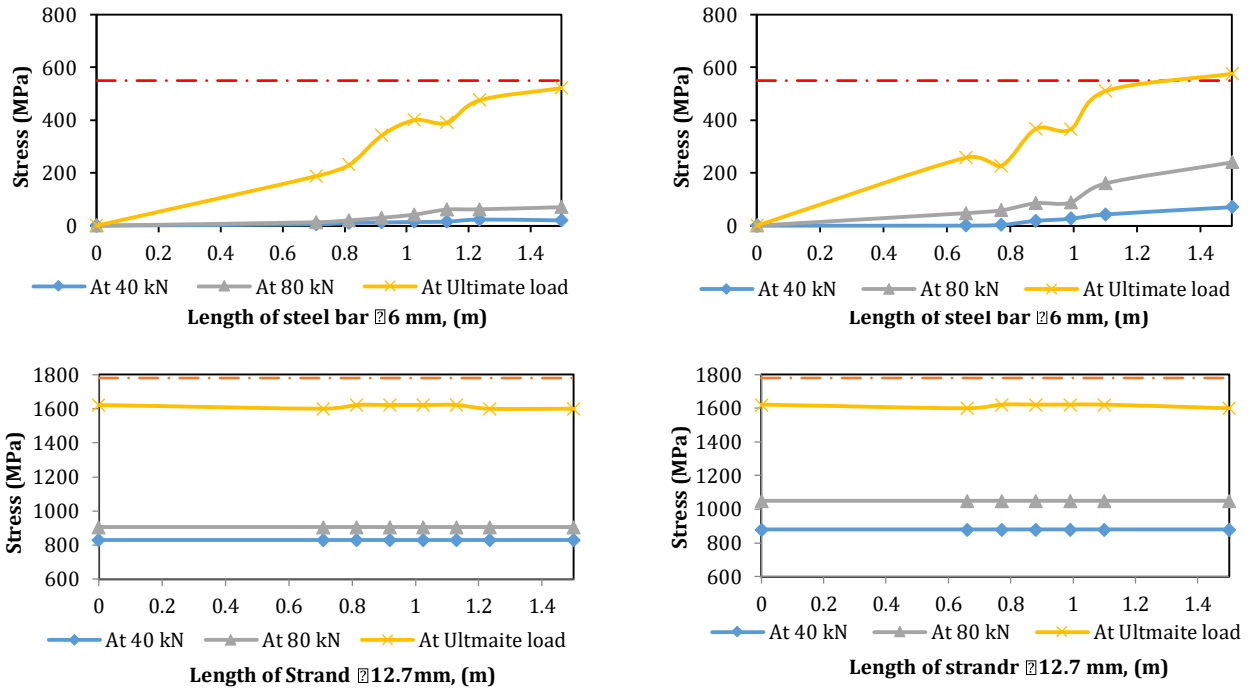

a) PQ8 beam **b) PQI8**

Figure 17. Distribution of stresses in flexural steel reinforcements of investigated beams**.**

5. CONCLUSIONS

This work presents a damage plasticity model (CDPM) as a numerical non-linear FE to simulate existing non-prismatic prestressed concrete beams with different shapes of multi-openings. The tested specimens were numerically validated until a satisfactory degree of precision was reached by realizing a good FE modelling technique and entirely accurate material modes. Accordingly, the following conclusions can be drawn:

- The CDPM model was an appropriate method to simulate concrete tension cracking and crushing. So, 3D non-linear FE models were developed to evaluate the RC elements' efficacy with the CDPM model. All potential nonlinearities, namely materials and geometrics, were considered in the created FE model.

- The 3D nonlinearity FEM described was then used to model multi-openings of different shapes for prestressed concrete hunched beams. The FE model successfully estimated failure load, the concrete crack growth caused by tension, the stress in steel reinforcement, and mid-span deflection in the prestressed concrete beams.

- The average ratios of loads and displacement at failure between experimentally tested rafters and simulations models were 0.98 and 0.97, respectively. The outcomes indicate that the FE models, when acted with a suitable FE modelling technique and accurate constitutive substance model, are highly successful in representing the nonlinearity behaviour of prestressed concrete hunched beams with different shapes of multi-openings.

- The parameterized nonlinearity FE analysis is an investigative approach that is very dependable. It is preferred because of the challenges, time-saving, budget, and labour involved in an experimental test.

REFERENCES

ABAQUS, A., 2013. ABAQUS Analysis User's Manual Version 6.13. Assault Systems.

Abdulkareem, B., and Izzet, A.F., 2022. Serviceability of Post-fire RC Rafters with Openings of Different Sizes and Shapes. *Journal of Engineering*, 28(1), pp. 19-32. Doi.org/10.31026/j.eng.2022.01.02

ACI Committee 318, 2019. Building code requirements for structural concrete (ACI 318M-19) and commentary (318R-19). American Concrete Institute, Farmington Hills, Michigan. USA.

Al-Hilali, A. M., Izzet, A. F., and Oukaili, N., 2022a. Static Shear Strength of a Non-Prismatic Beam with Transverse Openings. *Engineering, Technology & Applied Science Research*, 12(2), 8349-8353. Doi.org/10.48084/etasr.4789

Al-Hilali, A.M., Izzet, A.F., and Oukaili, N.K., 2022b. Deformability of non-prismatic prestressed concrete beams with multiple openings of different configurations. *Journal of the Mechanical Behavior of Materials*, 31(1), pp. 118-126. Doi.org/10.1515/jmbm-2022-0013

Alkhafaji, F.J., and Izzet, A.F., 2020, July. Experimental and Numerical Comparison of Prestressed Perforated Concrete Rafters of Different Configurations. IOP Conference Series: Materials Science and Engineering, 888(1): (P. 012080). Doi 10.1088/1757-899X/888/1/012080

Alkloub A, Allouzi R. Naghawi H., 2019. Numerical non-linear buckling analysis of tapered slender reinforced concrete columns. *International Journal of Civil Engineering*. 17(8), pp.1227-40. Doi: 10.1007/s40999-019-00395-5

Al-Shaarbaf, A.S., Al-Bayati, N.A.M.J. and Al-Kaisy, D.I., 2007. Nonlinear finite element analysis of reinforced concrete beams with large opening under flexure. *Eng Technol*, *25*(2), pp .210-228.

Amiri, J.V. and Alibygie, M.H., 2004, August. Effect of small circular opening on the shear and flexural behavior and ultimate strength of reinforced concrete beams using normal and high strength concrete. In *Proceedings of the 13th World Conference on Earthquake Engineering, Vancouver, BC, Canada* (Vol. 18).

Demir, A., Ozturk, H., and Dok, G., 2016. 3D Numerical Modeling of RC Deep Beam Behavior by Non-linear Finite Element Analysis. *Disaster Science And Engineering*, 2(1), pp. 13-18.

Esfahani, M.H., Hejazi, F., Vaghei, R., Jaafar M.S.B., and Karimzade, K., 2017. Simplified damage plasticity model for concrete. *Structural Engineering International*, 27(1), pp. 68-78. Doi:10.2749/101686616X1081

Hassan, M.A.J., and Izzet, A.F., 2019a. Serviceability of reinforced concrete gable roof beams with openings under static loads. *Engineering, Technology & Applied Science Research*, 9(5), pp. 4813-4817. Doi.org/10.48084/etasr.3110

Hassan, M.A.J., and Izzet, A.F., 2019b. Experimental and numerical comparison of reinforced concrete gable roof beams with openings of different configurations. *Engineering, Technology & Applied Science Research*, 9(6), pp. 5066-5073. Doi.org/10.48084/etasr.3188

Hognestad, E., 1951. A study of Combined Bending and Axial Load in R.C. Members. M.Sc. Thesis, Civil Engineering Department, University of Illinois Engineering Exp. Sta. Bull. No.399.

Hou, C., Matsumoto, K., and Niwa, J., 2015. Shear failure mechanism of reinforced concrete haunched beams. Journal of JSCE, 3(1), pp. 230-245. DoiI:10.2208/journalofjsce.3.1_230

Huang, Y., Kang, T.H.K., and Ramseyer, C., and Rha, C., 2010. Background to multi-scale modelling of unbounded Post-Tensioned concrete structures. *Int. J. Theoretical and Applied Multiscale Mechanics*, 1(3), pp. 219-235. Doi.org/10.1504/IJTAMM.2010.033601

Jankowiak, T., and Odygowski, T., 2005. Identification of Parameters Of Concrete Damage Plasticity Constitutive Model. *Foundation of Civil and Environmental Engineering*, No. 6, pp.53-69.

Kmiecik, P., and Kamiēski, M., 2011. Modelling of reinforced concrete structures and composite structures with concrete strength degradation taken into consideration. *Archives of Civil and mechanical engineering*, XI(3), pp. 623–636. Doi:10.1016/S1644-9665(12)60105-8

Lubliner, J., Oliver, J., Oller, and S., Oñate, E., 1989. A plastic-damage model for concrete. *International Journal of solids and structures*, 25(3), pp. 299-326. Doi:10.1016/0020-7683(89)90050-4

Madkour, H., and Ahmed, K., 2007. Three-dimensional modelling for reinforced concrete beams with openings based on nonlinear elastic-damage theory. *JES. Journal of Engineering Sciences*, *35*(1), pp.9-27. Doi: 10.21608/JESAUN.2007.111370

Mansur, M.A., Lee, Y.F., Tan, K.H., and Lee, S.L., 1991. Tests on RC continuous beams with openings. Journal of Structural Engineering, 117(6), pp. 1593-1606. Doi.org/10.1061/(ASCE)0733-9445(1991)117:6(1593)

Mansur, M. A., and Tan, K. H., 1999. Concrete beams with openings: analysis and design (Vol. 20). CRC Press.

Naik, P.K., and Manjunath, M., 2017. Pushover analysis of multi-storey frame structure with haunched beam. *International Journal of Trend in Research and Development*, 4(3), pp. 333-336.

Oukaili, N.K., and Shammari, A.H., 2013, December. Response of reinforced concrete beams with multiple web openings to static load. *Fourth Asia-Pacific Conference on FRP in Structures, Melbourne, Australia*. Doi:10.1260/1369-4332.17.12.1747.

Park, R., and Paulay, T., 1975. Reinforced Concrete Structures, Wiley, NY, USA.

Reddiar M.K.M., 2009. Stress-strain model of unconfined and confined concrete and stress-block parameters. MSc. Thesis, Civil Engineering Department, Texas A & M University.

Sahi, A.M. and Abd Ali, M.S., 2021. Experimental Study of Hollow Slender Reinforced Concrete Columns Subjected to Eccentric Loads. *Civil and Environmental Engineering*, *17*(1), pp. 303-317. Doi.org/10.2478/cee-2021-0032

Salam, S.A., 1977, August. Beams with openings under different stress conditions. Proceedings of 3rd Conference on Our World in Concrete and Structures, CI-Premier, Singapore, 25-26 Aug., 259-267.

Samir, P. S., 2013. Precast Prestressed Concrete Truss-Girder for Roof Applications. MSc Thesis, University of Nebraska, Lincoln.

Scott, B.D., Park, R., and Priestly, M.J.N., 1982. Stress-strain behavior of concrete confined by overlapping hoops at low and high strain rates. *ACI Structural Journal*, 79(1), pp. 13-27. **Doi:**10.14359/10875

Seow, P.E.C., and Swaddiwudhipong, S., 2005. Failure surface for concrete under multiaxial load –a unified approach. *Journal of Materials in Civil Engineering*, 17(2), pp. 219-228. Doi:0.1061/(ASCE)0899-1561(2005)17:2(219)

Tu'ma, N.H., Aziz, M.R., and Barry, H.J., 2021. Residual Tensile Stress Estimation for Shear Strength of UHPC Nonprismatic Beams. *Civil and Environmental Engineering*, 17(1), pp. 164-177. Doi:10.2478/cee-2021-0017

Wang, T., Hsu, T.T.C., 2001. Non-linear finite element analysis of concrete structures using new constitutive models. *Computers and Structures*, 79(32), pp. 2781-2791. Doi.org/10.1016/S0045-7949(01)00157-2